Supplementary material to:

R. Parboosing, T. Govender, G.E.M. Maguire and H.G. Kruger,

Synthesis, Characterization and Biocompatibility of a Multifunctional Gold Nanoparticle System for the Delivery of Single-Stranded RNA to Lymphocytes,

S. Afr. J. Chem., 2018, **71**, 1–14.

Supplementary Material

Appendix A: Confirming PEGylationby Gel Electrophoresis and Colloidal Stability Test

PEGylation of the multifunctional nanoparticle is essential to ensure its stability in physiological solutions.[1] Successful PEGylation was conveniently determined by the Colloidal Stability Test, in which the colour of a solution of bare (non-PEGylated) gold nanoparticles rapidly changes from wine red/pink to purple in the presence of high salt concentrations (indicating the formation of aggregates). PEGylated nanoparticles are stable in solutions containing high concentration of salts, and do not undergo any visible colour change (Figure S1).

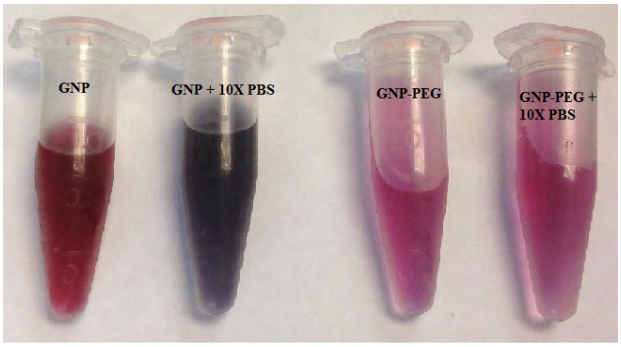

Figure S1: Colloidal Stability Test: A 1 ml solution of bare gold nanoparticles (GNP), rapidly changes to a purple colour upon the addition of 100 µL 10x PBS (GNP + 10x PBS), while PEGylated gold nanoparticles (GNP-PEG) do not (GNP-PEG + 10x PBS).

Successful PEGylation may also be confirmed visually on gel electrophoresis since bare citrate capped gold nanoparticles are negatively charged[2] while PEGylated gold nanoparticles are neutral (Figure S2). A 2 % agarose gel was prepared with TBE (Tris/Borate/EDTA) buffer (pH = 8.3). A 10 µL aliquot of nanoparticle solution was mixed with an equal volume of 40% w/v sucrose and then loaded into the well of the agarose gel. The gel was run for 40 minutes at 120 V. A sufficiently high concentration of gold nanoparticle solution was used to permit visualisation and photography of the “bands” on the gel.

Gel electrophoresis was also performed to confirm conjugation of RNA to gold nanoparticles i.e. to show that the fluorescent bands (RNA) co-localised with visible gold nanoparticle bands. However, fluorescence was not observed, probably due to the low number of RNA molecules per gold nanoparticle and surface quenching of the fluorescence signal.

Figure S2: Gel electrophoresis of gold nanoparticles showing migration of negatively charged bare gold nanoparticles towards the positive pole. PEGylated gold nanoparticles (left lane) and PEGylated gold nanoparticles with SPDP linker molecule (right lane) have a neutral charge and do not migrate.

Appendix B: Peptide Synthesis[3]

Design of the Peptide Ligand: Targeting CD4 Cells

A synthetic peptide, that specifically binds the CD4 receptor, was attached to the gold nanoparticle to potentially enhance receptor-mediated endocytosis and uptake of the nanoparticle by CD4+ MT4 lymphocytes. The design of the peptide was based on systematic exploration of the variable domains of an anti-CD4 mAb by the "Spot" method.[4-8] This peptide has been shown to cause dose dependent inhibition of IL2 secretion by CD4+ cells, inhibition of HIV-1 promoter activation, specific, dose-dependent binding to soluble CD4 in an ELISA assay and dose-dependent inhibition of binding to soluble CD4 by anti-CD4 mAb in an ELISA inhibition assay.[5] An AAC "tail" links the peptide to the polyethyleneimine via an SPDP linker molecule. The peptide was synthesized by routine FMoc Solid Phase Synthesis[3, 9-12] on a CEM microwave peptide synthesizer[13-14] and cyclised by on-resin iodine-oxidation of cysteine residues close to the N and C termini of the peptide.[7, 15]

Reagents

9-fluorenylmethoxycarbonyl (FMoc) protected amino acids and coupling reagents were purchased from GLS Biochem Systems. Solvents were purchased from Sigma-Aldrich.

Peptide Sequence

The sequence of the peptide is as follows:**KC*LTTFGVHWVRQSC*KAAC$^{\#}$**. The peptide consists of 10 (~53%) hydrophobic, 4 (~21%) polar, 4 positively charged and 0 negatively charged amino acids.[16]The "inner" cysteines that are involved in the cyclization reaction, are shown as C*, and the "tail" cysteine that links to the gold nanoparticle surface is shown as C$^{\#}$.

Solid PhasePeptide synthesis

FMoc Solid Phase Peptide synthesis was carried out in a C to N direction on a CEM microwave peptide synthesizer at a 0.1 mmol scale. Rink amide resin was used as the solid support system.[13-14]Deprotection was achieved by 20% piperidine/DMF(dimethylformamide)(v/v)[13, 17] and coupling by 1:1:1 amino acid/HBTU(N-[1H-benzotriazol-1-yl)(dimethylamino)methylene]-N-methyl-methanaminium hexafluorophosphate N-oxide)/ DIPEA (N,N-diisopropyl ethylamine) in DMF.[13]Table S1 provides the details of side chain protection/deprotection strategy, while Table S2 lists the microwave synthesis conditions. DMF washes were performed between the deprotection and coupling steps.

Table S1: Side Chain Protection/Deprotection[3, 11]

# (L-R)	Amino Acid	Letter (label)	Symbol	Protection	Deprotection
1	Lysine	**K**	Lys	Mtt	95%TFA
2	Cysteine	**C***	Cys	Mmt	1% TFA
3	Leucine	**L**	leu	NONE	NONE
4	Threonine	**T**	Thr	tBu	95%TFA
5	Threonine	**T**	Thr	tBu	95%TFA
6	Phenylalanine	**F**	Phe	NONE	NONE
7	Glycine	**G**	Gly	NONE	NONE
8	Valine	**V**	Val	NONE	NONE
9	Histidine	**H**	His	Trt	95%TFA
10	Tryptophan	**W**	Trp	Boc	95%TFA
11	Valine	**V**	Val	NONE	NONE
12	Arginine	**R**	Arg	Pbf	95% TFA
13	Glutamine	**Q**	Gln	Trt	95% TFA
14	Serine	**S**	Ser	tBu	95%TFA
15	Cysteine	**C***	Cys	Mmt	1% TFA
16	Lysine	**K**	Lys	Boc	95%TFA
17	Alanine	**A**	Ala	NONE	NONE
18	Alanine	**A**	Ala	NONE	NONE
19	Cysteine	**C#**	Cys	Trt	95% TFA

Boc tert-butoxycarbonyl, **Mmt** 4-methoxytrityl, **Pbf** 2,2,4,6,7-pentamethyldihydrobenzofuran-5-sulfonyl, **Pmc** 2,2,5,7,8-pentamethylchroman-6-sulfonyl, **tBu** tert-butyl, **TFA** trifluoroacetic acid, **Trt** triphenylmethyl (trityl), **C*** "inner" cysteines **C#** "tail" cysteine

Table S2: Microwave Conditions for Coupling/Deprotection[13-14]

	Power (Watts)	Temperature (°C)	Time (s)
Single Coupling (all amino acids except arginine) 30 Minute coupling	0	25	900
	35	73	900
Arginine Coupling 60 minutes (double coupling)	0	25	2700
	35	73	900
De-protection	40	73	180
Total Run Time	26 hours		

On Resin Cyclization[15, 18-19]

To avoid side-reactions, cyclization was performed on resin with the N-terminal amino acid still protected with the FMoc group. A disulphide bond was formed between two the cysteine residues (C*) at positions 2 and 15, by iodine-oxidation. The details of the procedure are as follows:

1. The resin was swelled with DMF (3x).
2. Mmt was cleaved from the "inner" cysteines using 1% TFA.
3. The peptide was oxidized with I_2 (10 eq) in DMF for 1.5 hours, with gentle stirring at room temperature.
4. The resin was washed thoroughly with DCM (dichloromethane) (5x), CCl_4 (5x) and DMF (10x) to remove iodine.
5. Peptides were cleaved from the resin and the remaining side chain protecting groups removed with 1% TIS(tri-isopropylsilane) + 1% thioanisole + 1% 1,2 ethanedithiol + 95% TFA in DCM for 2 hours.[13]

The peptides were purified on a Younglin ACME 9000 instrument using an ACE C-18 reverse phase semi-preparative High Performance Liquid Chromatography (HPLC) column and mass spectra were obtained on a Bruker ESI-QTOF mass spectrometer and Shimadzu Prominence LC-MS System. The purified peptide was lyophilized using a VirTis benchtop K freeze dryer and stored at -20°C until use.

Linker Conjugation

SPDP is an amine-sulfhydryl crosslinking molecule that has an amine reactive portion (*N*-hydroxysuccinimide (NHS) ester) and a sulfhydryl-reactive portion (2-pyridyldithio group)

The 2-pyridyldithio group reacts optimally with sulfhydryl- containing molecules, such as cysteine, between pH 7 and 8. The cysteine at the end of the "AAC" tail of the cyclic peptide was conjugated to SPDP as follows:

25µL of 20mM SPDP solution was added to 2 mg cyclic peptide dissolved in 1 mL of PBS. The mixture was incubated for 30 minutes at room temperature. Excess SPDP was then removed by Sephadex G-25 PD-10 desalting column (GE Healthcare Life Sciences, Pittsburgh, Pennsylvania, USA). Then the solution was added to 1 mL polyethyleneimine coated gold nanoparticle and incubated overnight to allow conjugation of the peptide-SPDP with the amine side chains of polyethyleneimine via the NHS ester of SPDP. The excess peptide-SPDP was removed by repeated centrifugation and washing with PBS.

Appendix C: Aggregation and its quantification by Light Microscopy and Photographic Software

Nanoparticle aggregation is often overlooked or understated; however, the complexity of the mechanisms and factors involved, and the importance of the phenomenon, are now being recognised.[1] In this study, it is postulated that aggregation occurs whenseveral nanoparticles are attracted to the same polyethyleneimine molecule.[20] The proposed mechanism is shown in Figure S3.

Aggregation may be detected by colour change, spectrophotometry, dynamic light scattering, nanoparticle tracking analysis[21] and microscopy (electron or light). In this study, light microscopy was found to be a convenient method to quantify aggregation since it is quick, inexpensive, can be performed *in situ* (without requiring transfer of the sample to a cuvette), does not destroy or disturb the sample (so that incubation can be continued and the measurement repeated at varying points of time).It requires a small sample volume and has no limit in terms of size and shape of the particles. Moreover, it is unlikely that particles larger than 1 micron will be internalised, and 1 micron is incidentally the approximate maximum resolution of a light microscope (at 100x magnification). Additionally, it is the total number of nanoparticles contained within the sum of all aggregates that is of concern (since these may no longer be taken up), rather than the number of aggregates, (a large number of small aggregates may contain the same number of nanoparticles as a small number of large aggregates). The number of nanoparticles contained within an aggregate is directly proportional to its total volume. Furthermore, if the assumption is made that aggregates are formed and orientated randomly in three dimensional space, then the surface area is directly proportional to the volume of the aggregate and hence to the total the number of nanoparticles contained within it. Therefore, a two dimensional photograph of aggregates under light microscopy will be a good approximation of the total number of aggregated gold nanoparticles.

It must be noted that the assumption that number of particles within an aggregate is linearly proportional to its size (and mass) cannot be taken for granted, and is certainly not true if aggregates are formed as self-similar (mass-fractal) structures, in which case power-law (rather than linear) relationships are characteristic.[1] Nevertheless, in the absence of certainty about the exact mechanism of aggregation (and the effect of “external forces”), such assumptions can only be tested by quantification within a defined experimental setup. Findings may certainly not be extrapolated to experimental setups where the conditions are different, even if such differences are seemingly minor.

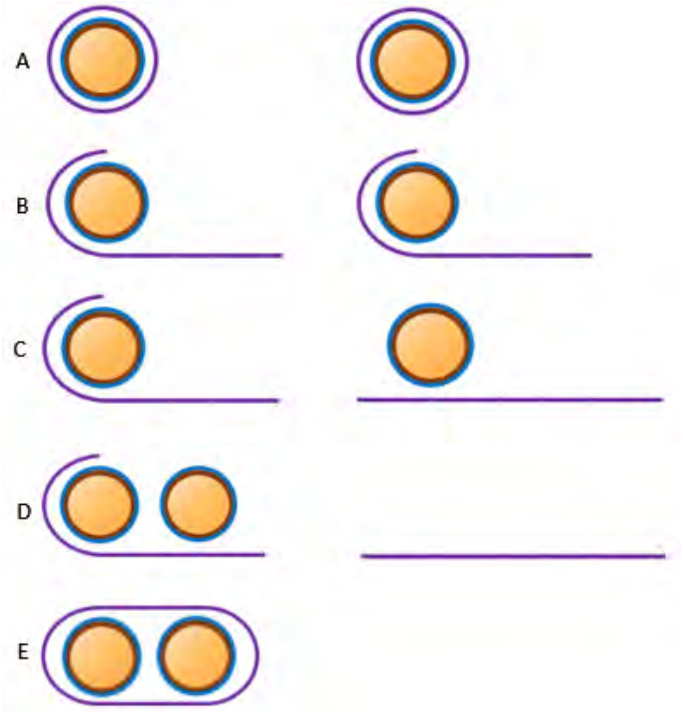

Legend

Negatively charged gold nanoparticle

Positively charged polyethyleneimine

Figure S3:Aggregation occurs when several nanoparticles are attracted to the same polyethyleneimine molecule.[20, 22-25]A. Non-aggregated gold nanoparticles coated with polyethyleneimine. Exposure to serum proteins is hypothesised to result in leeching of polyethyleneimine from the surface of nanoparticles (B, C). This results in the disorderly and random association of several (>1) nanoparticles with the same molecule of polyethyleneimine, resulting in the formation of aggregates (D, E). The polyethyleneimine used in this paper is branched but is shown here as a linear molecule for simplicity. The aggregates shown here (D and E) consists of 2 nanoparticles (a doublet); the number of nanoparticles contained in aggregates described in this paper is unknown, but is most likely much larger and variable.

Quantification of aggregation by light microscopy was performed as follows

1. Aliquots of the nanoparticle solutions weredispensed in triplicate into the well of a clear flat-bottomed microtiter plate.
2. The wells were then viewed under a Leica DMIL light microscope (Leica, Wetzlar, Germany) at 200x magnification.
3. Light intensity and course focus were fixed during observation to avoid well to well variation in viewing conditions.
4. Representative images were captured on a Zeiss Axiocam 105 camera (Carl Zeiss, Oberkochen, Germany).
5. The images were imported into Image J software in an 8-bit grayscale format.
6. The black:white threshold was adjusted by the maximum entropy method.[26]The choice of threshold adjustment method was made empirically. The method that most accurately represented the percentage of black pixels that corresponded to visual approximation was chosen. The important point is that data using different methods cannot be compared. Therefore, the method, once chosen, was used for all experiments in which data was compared.
7. The number of black pixels (representing aggregated nanoparticles) was enumerated by Image J software and expressed as a percentage of the total number of pixels.
8. In order to generate a standard curve, serial, 2-fold dilutions of a highly aggregated gold nanoparticle solution were made with PBS, in the wells of a clear, flat bottom microtiter plate. The solution was thoroughly mixed at each step to ensure that aggregated nanoparticles were likewise diluted. Dilutions were prepared in triplicate. Photographs were taken of each dilution and the percentage black pixels was determined as described above (steps 1-7). The percentage black pixels was plotted against serial dilutions of the aggregated gold nanoparticle (log transformed to base 2) (Figure S4). The method showed excellent correlation ($r = 0.99$) between percentage black pixels vs. actual aggregation of serially diluted aliquots in the range of 0.3 to 50 % aggregation. Typical images are shown in Figure S5.

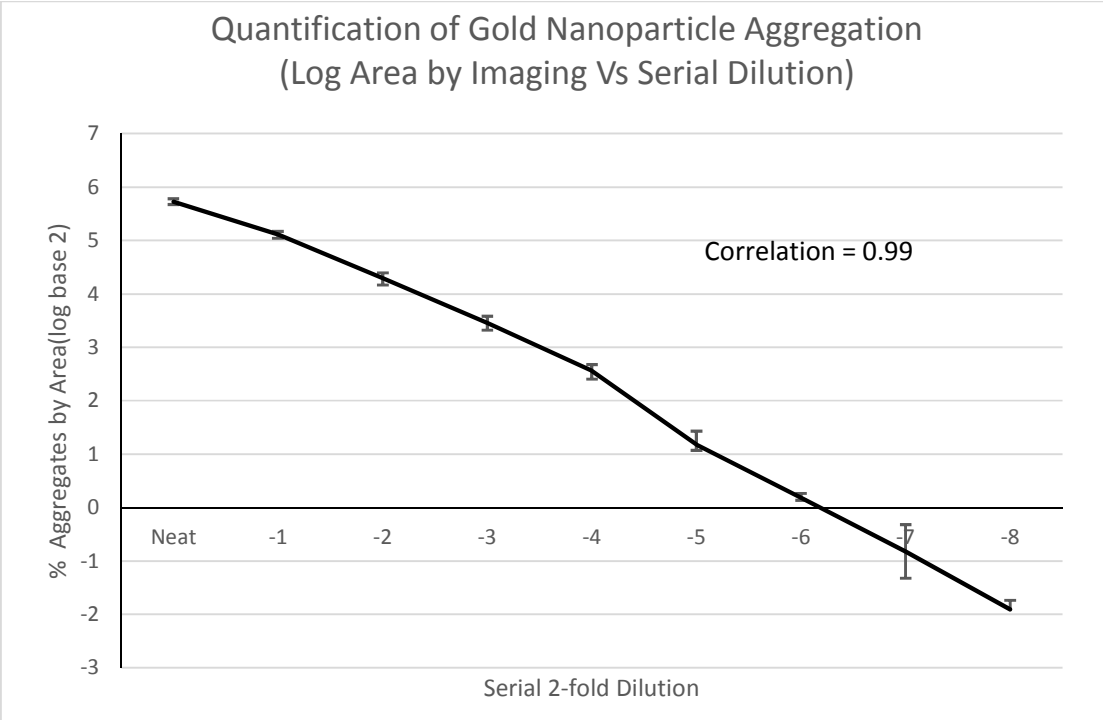

Figure S4:Graph showing linear relationship between serially diluted aggregated gold nanoparticles and photographically determined aggregation (expressed as a percentage of black pixels)

Dilution	Original image (200x)	Grayscale/threshold adjusted	% black pixels
1	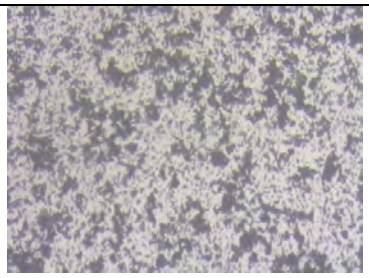	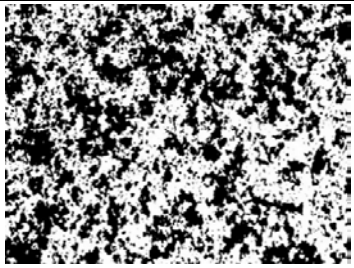	45.9%
½	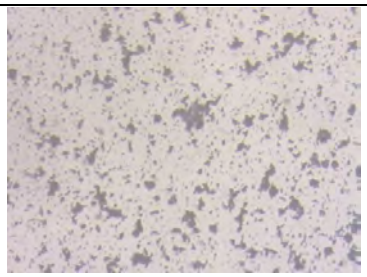	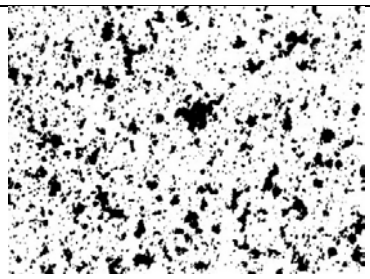	20.09%
¼	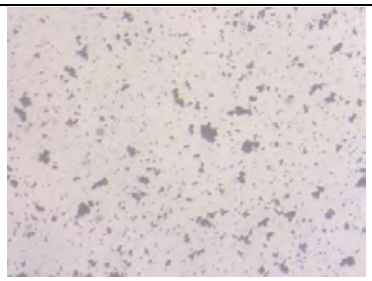	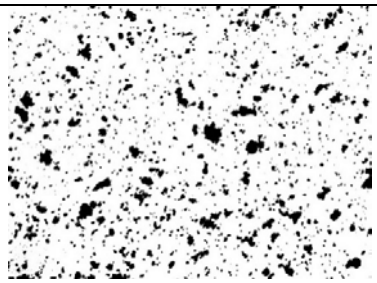	11.8%
⅛	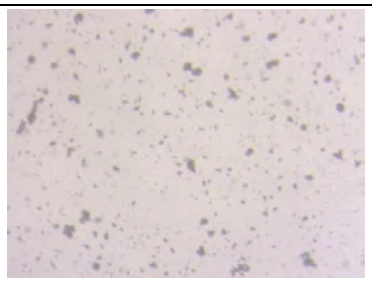	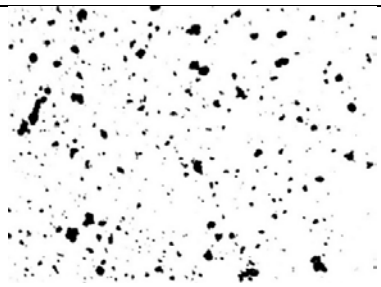	5.5%
1/16	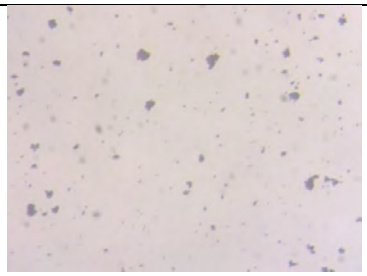	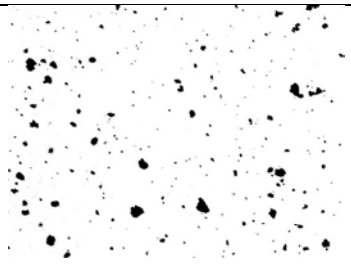	2.9%

Figure S5:Representative images of serially diluted aggregated nanoparticles under 200x magnification, the corresponding 8-bit grayscale images with the black-white threshold adjusted by the maximum entropy method, and the percentage black pixels (as determined by ImageJ software).

Appendix D: SPDP Loading

The loading (SPDP linker molecules per nanoparticle) was determined by measuring the concentration of pyridine-2-thione which is released from the surface of the gold nanoparticle when exposed to the reducing agent dithiothreitol (DTT).

The assay is performed as follows:

1. SPDP was conjugated to the PEGylated nanoparticle as described in the synthesis section. For the purposes of this experiment, the volume of SPDP and PEGylated gold nanoparticle used in the reaction was increased (without altering the concentration of the reactants) so that a "measurable" concentration of pyridine-2-thione would be released at the end of the assay. A "measurable" concentration of pyridine-2-thione was defined by an absorbance reading at least 3 standard deviations greater than the "Blank". In a typical experiment, 20 mL of reaction product (i.e. a mixture of 10 mL SPDP + 10 mL GNP-PEG), re-suspended after final centrifugation to a volume of 1mL, was sufficient. It is important that the volume of the reaction mixtures be adjusted, rather than the concentration of SPDP. SPDP is poorly soluble in water; increasing the concentration excessively results in precipitation and spurious results.
2. At the end of the reaction described in step one, the solution was repeatedly washed by centrifugation and resuspension in PBS-Tween-20™ (0.01%) to remove excess SPDP. A 500 µL aliquot of the supernatant after the last spin was tested for the presence of SPDP using the pyridine-2-thione assay (as described in the steps below). An absorbance value of < 0.01 (or a reading within 1 standard deviation of the "Blank") was regarded as suitable. Typically, 4 washes were required for adequate removal of excess SPDP.
3. After the last wash, the gold nanoparticle solution (GNP-PEG-SPDP) was re-suspended in 1 mL PBS/Tween, vortexed thoroughly, and then divided into 2 x 500 µL aliquots.
4. 1 aliquot of the gold nanoparticle solution was mixed with 5 µL PBS (labelled GNP-PBS); the other aliquot of the gold nanoparticle solution (labelled GNP-DTT) was mixed with 5 µL DTT (15 mg/mL).
5. The mixed solutions were incubated at room temperature for 15 minutes.
6. After exactly 15 minutes, the aliquots were centrifuged until the supernatant was clear and the gold nanoparticle formed a distinct pellet.
7. The absorbance at 343nm of the supernatant of each aliquot was recorded in triplicate.

8. The difference in absorbance was calculated as follows:
   Difference in absorbance = GNP-DTT – (GNP-PBS)
   Where GNP-DTT = mean absorbance of supernatant of GNP solution treated with DTT
   GNP-PBS = mean absorbance of supernatant of GNP solution treated with PBS
   PBS-TWEEN was read as “Blank”.
9. The molar concentration of the SPDP was then calculated as follows:
   Molar concentration (in mM) = difference in absorbance ÷ (8.08 $mM^{-1}cm^{-1}$ x path-length in cm), where 8.08 x $10^{-3}M^{-1}cm^{-1}$ is the“extinction coefficient” or molar absorptivity for pyridine-2-thione at 343 nmand the path-length, when using the BioSpec Nano in the 0.7 mm mode.

In a typical experiment, the molar concentration of pyridine-2-thione in the final 1 mL aliquot was found to be 407 µM or 407 000 nM (based on mean absorbance difference of 0.23 units). The concentration of gold nanoparticle in the same aliquot was 20nM (as determined by absorbance measurements).[27] Therefore, each nanoparticle was decorated with an average of (407 000 ÷ 20 =) 20350 SPDP linker molecules (or ~2.6 SPDP molecules per nm^2 nanoparticle surface area).

Appendix E: Details of the Method to Determine RNA Concentration to Calculate Loading and Uptake

It was necessary to measure the concentration of RNA to allow for the determination of RNA loading per nanoparticle and to assess cellular uptake (as an alternative to flow cytometry and epifluorescent microscopy). The RNA was synthesised with a fluorescein tag at the 3' end, which allows for quantification by generation of a standard curve of fluorescence. This was measured as relative fluorescence units (RFU vs. RNA concentration and determined by absorbance and serial dilutions; a representative graph is presented in Figure S6. Fluorescence is significantly more sensitive than absorbance for RNA quantification. The approximate lower limit for absorbance-based quantification using the Biospec Nano is given as 15 ng/µL of ds DNA based on the 0.7 mm path length method. This equates to a limit of quantification of RNA used in this experiment to approximately 2.8 µM. By contrast, measurement by fluorescence (using the method described in this section) is at least 1000x more sensitive which allows quantification in the nanomolar range (from as low as 1 nM).

The concentration of the stock RNA (which was synthesised in the micromolar scale) was determined by UV spectroscopy on the BioSpec Nano. An adjustment was made for the absorbance of fluorescein using the on-board software. The ratio of absorbance at 260nm to absorbance at 280nm allows for the determination of the concentration of RNA using the Beer-Lambert Law.[28]The concentration of a typical aliquot of RNA using this method was determined to be 888 ng/µL. The molecular weight of the RNA = 5315g/mol or 5315ng/nmol. Therefore, the concentration of the RNA = 888/5315 nmol/µL = 167µmol/L = 167µM.

The concentration was adjusted to 10µM by addition of RNAse free deionised water. Eight serial 10 fold dilutions were made, in triplicate, in a black microtiter plate and the fluorescence read in the Glomax Multimode Detection System using the Blue filter (Excitation 490nm/Emission 510-570nm). The readings were log transformed (base 10) and plotted in Excel™ and the RNA concentration then determined by linear extrapolation on the logarithmic scale.

For determination of RNA loading, the concentration of released RNA was determined (e.g. 1200nM) and divided by the concentration of gold nanoparticle (e.g. 1.14 nM) to yield the number of strands of RNA per gold nanoparticle (e.g. 1053).

To determine uptake, the concentration of RNA was similarly determined in the supernatant following cell lysis and centrifugation. The concentration of RNA (e.g. 75nM) was then used to calculate the

number of nanomoles of RNA per million cells (e.g. 7.5 x 10^{-5} nmoles per million cells) which corresponds to 45 000 strands of RNA per cell.

The limit of detection of RNA uptake per cell was calculated based on the lower limit of detection of RNA of 1nM, corresponding to a Relative Fluorescence Units (RFU) = 5.3. Moreover, RFU values <7 (i.e. falling within 2 standard deviations away from the mean) are likely due to instrument "noise" rather than biological factors. Therefore, only readings > 7 RFU above the mean were regarded as significant. The standard deviation of the fluorescence measurements was calculated by reading 30 wells of a "blank" plate.

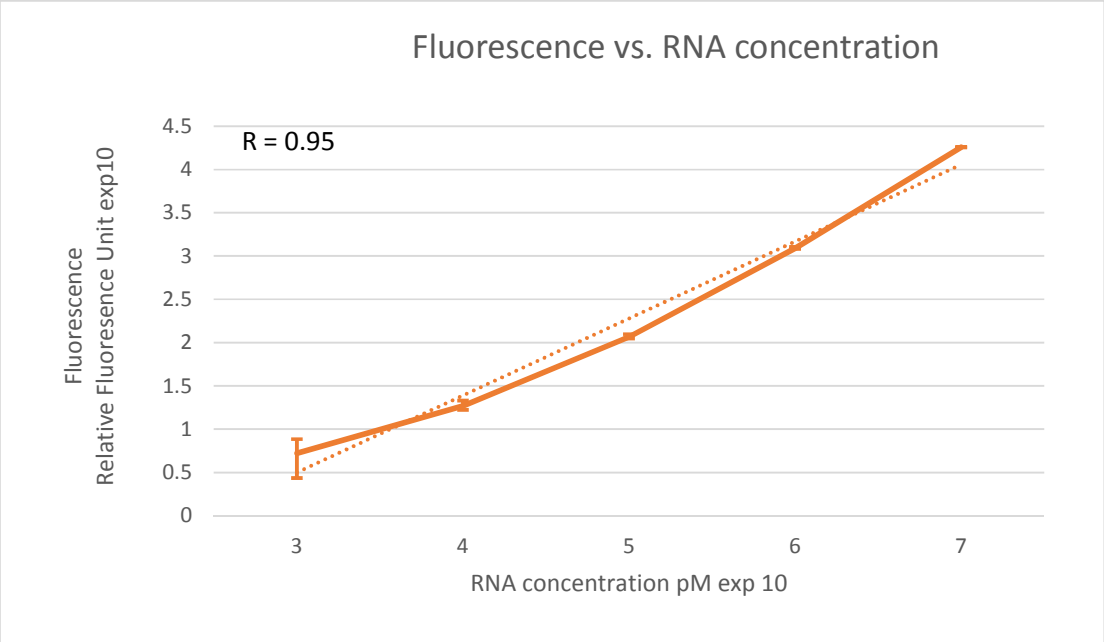

Figure S6:Graph showing log-linear relationship between RNA concentration (in pM) and relative fluorescence units (dimensionless) over a wide range (from about 1 nM to 10 µM). Fluorescence readings of RNA below 1 nM concentration were close to zero and are not shown. The dotted line is the linear trend line.

Appendix F: Optimisation

A series of experiments were carried out, in which the synthesis procedure and uptake conditions were varied, in an attempt to improve aggregation and uptake.

Size of GNP

In a previous study to determine the effect of nanoparticle size on uptake into Hela cells, nanoparticles with diameter 30–50 nm were taken up more readily than smaller or larger particles.[29] Therefore, the assumption was made that the nanoparticles used in this paper (30-40nm) would achieve similar results. Nevertheless, the synthesis procedure (as described in the Synthesissection) was repeated with nanoparticles of diameter 15nm, without significant improvement in aggregation and uptake. Nanoparticles of size 15nm were synthesised using the same method as described for 30-40 mm gold nanoparticles, except that the amount of sodium citrate was doubled.[30] The concentration of reagents for each of the subsequent steps was adjusted to take into account the surface area of 15nm particles.

RNA concentration

It is important to optimise the conjugation of the RNA to the gold nanoparticle, since synthetic RNA is expensive and produced in small quantities (usually in the nanomolar or micromolar scale). The proportion of RNA that binds to the surface of the nanoparticle (as opposed to the RNA that fails to bind) was determined by measuring the concentration of the RNA in the supernatant pre and post reaction.

In a typical reaction, only ~1.2 µM of 15 µM (i.e. 8%) of RNA added per reaction, conjugated to the gold nanoparticle. The rest (92%) of the RNA remains in the supernatant. This was confirmed by measuring the concentration of the RNA in the supernatant, both by fluorescence and absorbance. Lee *et al.* do not explicitly determine the proportion of RNA that conjugates to the GNP.[31] However, they provide sufficient data for the calculation to be made. Based on reaction of 15 µM RNA and 30 nM GNP in 400 µL buffer and resulting ~30 strands of RNA per particle, the proportion of RNA conjugated to the surface of the GNP was calculated to be 6%. Therefore, the efficiency of RNA conjugation in our experiments is in keeping with that of Lee *et al.*[31] Increasing the concentration of RNA did not improve the loading.

Polyethyleneimine concentration

The concentration of polyethyleneimine optimised for coating in a previous study was 1 mg polyethyleneimine per mL.[23] It was not deemed viable to significantly reduce the concentration of

polyethyleneimine since a positively charged nanoparticle was required to facilitate cellular uptake. The zeta potential of the nanoparticle was only +13.5 mV, even when synthesised with polyethyleneimine at 1 mg/mL (compared to a zeta potential of ~+60 mV achieved by a layer-by-layer approach.[23] Increasing the concentration of polyethyleneimine (up to 10 mg/mL) resulted in an increase in zeta potential (~23.6 mV). However, the aggregation of the nanoparticleswas exacerbated and there was no improvement in the uptake (as determined by flow cytometry). Therefore, the optimal concentration of 1 mg/mL, as described by Elbakry *et al.*[23] was used in subsequent experiments.

Treatment Conditions

Uptake was optimal with treatment duration of 24 hours (compared to 1, 2 hours and 4 hours). The use of serum-free OptiMEM™ media did not improve uptake (as determined by epifluorescent microscopy). The experiments were repeated with an adherent cell line (a human cervical epithelial carcinoma cell line (Hela), obtainedthrough the NIH AIDS Reagent Program, Division of AIDS, NIAID, NIH: HeLa CD4(HT4-6C) from Dr Bruce Chesebro).[32-33] However, the nanoparticle was not taken up by this cell line (as determined by flow cytometry).

References

1. Moore, T. L.; Rodriguez-Lorenzo, L.; Hirsch, V.; Balog, S.; Urban, D.; Jud, C.; Rothen-Rutishauser, B.; Lattuada, M.; Petri-Fink, A., Nanoparticle colloidal stability in cell culture media and impact on cellular interactions. *Chemical Society reviews* **2015,***44* (17), 6287-305.
2. Giljohann, D. A.; Seferos, D. S.; Daniel, W. L.; Massich, M. D.; Patel, P. C.; Mirkin, C. A., Gold nanoparticles for biology and medicine. *Angew Chem Int Ed Engl* **2010,***49* (19), 3280-94.
3. Sewald, N.; Jakubke, H.-D., *Peptide Synthesis*. Wiley-VCH Verlag GmbH & Co. KGaA: 2009; p 175-315.
4. Monnet, C.; Laune, D.; Laroche-Traineau, J.; Biard-Piechaczyk, M.; Briant, L.; Bes, C.; Pugniere, M.; Mani, J. C.; Pau, B.; Cerutti, M.; Devauchelle, G.; Devaux, C.; Granier, C.; Chardes, T., Synthetic peptides derived from the variable regions of an anti-CD4 monoclonal antibody bind to CD4 and inhibit HIV-1 promoter activation in virus-infected cells. *J Biol Chem* **1999,***274* (6), 3789-96.
5. Bes, C.; Briant-Longuet, L.; Cerruti, M.; De Berardinis, P.; Devauchelle, G.; Devaux, C.; Granier, C.; Chardes, T., Efficient CD4 binding and immunosuppressive properties of the 13B8.2 monoclonal antibody are displayed by its CDR-H1-derived peptide CB1. *FEBS Lett* **2001,***508* (1), 67-74.
6. Bes, C.; Briant-Longuet, L.; Cerutti, M.; Heitz, F.; Troadec, S.; Pugniere, M.; Roquet, F.; Molina, F.; Casset, F.; Bresson, D.; Peraldi-Roux, S.; Devauchelle, G.; Devaux, C.; Granier, C.; Chardes, T., Mapping the paratope of anti-CD4 recombinant Fab 13B8.2 by combining parallel peptide synthesis and site-directed mutagenesis. *J Biol Chem* **2003,***278* (16), 14265-73.
7. Albericio, F., Developments in peptide and amide synthesis. *Curr Opin Chem Biol* **2004,***8* (3), 211-21.
8. Boschek, C. B.; Apiyo, D. O.; Soares, T. A.; Engelmann, H. E.; Pefaur, N. B.; Straatsma, T. P.; Baird, C. L., Engineering an ultra-stable affinity reagent based on Top7. *Protein Eng Des Sel* **2009,***22* (5), 325-32.
9. Wellings, D. A.; Atherton, E., Standard Fmoc protocols. *Methods Enzymol* **1997,***289*, 44-67.
10. Fields, G., Solid-phase peptide synthesis. *Molecular Biomethods Handbook* **1998**, 527-545.
11. Amblard, M.; Fehrentz, J. A.; Martinez, J.; Subra, G., Methods and Protocols of modern solid phase peptide synthesis. *Mol Biotechnol* **2006,***33* (3), 239-254.
12. Rapley, R.; Walker, J. M., *Molecular Biomethods Handbook*. 2nd ed.; Humana Press: Totowa, NJ, 2008; p xx, 1124 p.
13. Muthusamy, K.; Albericio, F.; Arvidsson, P. I.; Govender, P.; Kruger, H. G.; Maguire, G. E.; Govender, T., Microwave assisted SPPS of amylin and its toxicity of the pure product to RIN-5F cells. *Biopolymers* **2010,***94* (3), 323-30.
14. Pietersen, L. K.; Govender, P.; Kruger, H. G.; Maguire, G. E. M.; Wesley-Smith, J.; Govender, T., Peptide Functionalised Gold Nanoparticles: Effect of Loading on Aggregation and Proteolysis. *International Journal of Peptide Research and Therapeutics* **2010,***16* (4), 291-295.
15. Galanis, A. S.; Albericio, F.; Grotli, M., Enhanced microwave-assisted method for on-bead disulfide bond formation: synthesis of alpha-conotoxin MII. *Biopolymers* **2009,***92* (1), 23-34.
16. Guy, C. A.; Fields, G. B., Trifluoroacetic acid cleavage and deprotection of resin-bound peptides following synthesis by Fmoc chemistry. *Methods Enzymol* **1997,***289*, 67-83.
17. Fields, G. B., Methods for removing the Fmoc group. *Methods Mol Biol* **1994,***35*, 17-27.
18. Andreu, D.; Albericio, F.; Sole, N. A.; Munson, M. C.; Ferrer, M.; Barany, G., Formation of disulfide bonds in synthetic peptides and proteins. *Methods Mol Biol* **1994,***35*, 91-169.

19. Chen, L.; Annis, I.; Barany, G., Disulfide bond formation in peptides. *Curr Protoc Protein Sci* **2001,***Chapter 18*, Unit18 6.
20. Ariyawansa, T.; Pullman, H.; Amiji, M. M.; Bhavsar, M. M. D. The Development of Multifunctional Nanoparticles for Simultaneous Fluorescence Imaging and Gene Delivery. http://web.mit.edu/rsi/www/pdfs/papers/2006/2006-thilini.pdf.
21. James, A. E.; Driskell, J. D., Monitoring gold nanoparticle conjugation and analysis of biomolecular binding with nanoparticle tracking analysis (NTA) and dynamic light scattering (DLS). *The Analyst* **2013,***138* (4), 1212-8.
22. Wang, X.; Zhou, L.; Ma, Y.; Li, X.; Gu, H., Control of aggregate size of polyethyleneimine-coated magnetic nanoparticles for magnetofection. *Nano Research* **2010,***2* (5), 365-372.
23. Elbakry, A.; Zaky, A.; Liebl, R.; Rachel, R.; Goepferich, A.; Breunig, M., Layer-by-layer assembled gold nanoparticles for siRNA delivery. *Nano Lett* **2009,***9* (5), 2059-64.
24. Gittins, D. I.; Caruso, F., Tailoring the Polyelectrolyte Coating of Metal Nanoparticles. *The Journal of Physical Chemistry B* **2001,***105* (29), 6846-6852.
25. Schneider, G.; Decher, G., Functional core/shell nanoparticles via layer-by-layer assembly. investigation of the experimental parameters for controlling particle aggregation and for enhancing dispersion stability. *Langmuir* **2008,***24* (5), 1778-89.
26. Rasband, W. *Image J*, National Institutes of Health: 2016.
27. Haiss, W.; Thanh, N. T. K.; Aveyard, J.; Fernig, D. G., Determination of size and concentration of gold nanoparticles from UV-vis spectra. *Analytical chemistry* **2007,***79* (11), 4215-4221.
28. Thermo Fisher Scientific Inc. RNA quantitation is an important and necessary step prior to most RNA analysis methods. http://www.webcitation.org/6kdWpl2gs.
29. Chithrani, B. D.; Ghazani, A. A.; Chan, W. C., Determining the size and shape dependence of gold nanoparticle uptake into mammalian cells. *Nano Lett* **2006,***6* (4), 662-8.
30. Kanaras, A. G.; Wang, Z.; Hussain, I.; Brust, M.; Cosstick, R.; Bates, A. D., Site Specific Ligation of DNA Modified Gold Nanoparticles Activated by the Restriction Enzyme StyI. *Small* **2007,***3* (1), 67-70.
31. Lee, J. S.; Green, J. J.; Love, K. T.; Sunshine, J.; Langer, R.; Anderson, D. G., Gold, poly(beta-amino ester) nanoparticles for small interfering RNA delivery. *Nano Lett* **2009,***9* (6), 2402-6.
32. Chesebro, B.; Buller, R.; Portis, J.; Wehrly, K., Failure of human immunodeficiency virus entry and infection in CD4-positive human brain and skin cells. *Journal of Virology* **1990,***64* (1), 215-21.
33. Chesebro, B.; Wehrly, K., Development of a sensitive quantitative focal assay for human immunodeficiency virus infectivity. *Journal of Virology* **1988,***62* (10), 3779-88.